J Therm Anal Calorim (2016) 124:571–583
DOI 10.1007/s10973-015-5202-z

Elastic and anelastic relaxations accompanying relaxor ferroelectric behaviour of $Ba_6GaNb_9O_{30}$ tetragonal tungsten bronze from resonant ultrasound spectroscopy

Andrei Rotaru[1,2,3] · **Jason A. Schiemer**[2] · **Michael A. Carpenter**[2]

Received: 6 October 2015 / Accepted: 11 December 2015 / Published online: 6 January 2016

Abstract Tetragonal tungsten bronze (TTB) structures offer some promise as lead-free ferroelectrics and have an advantage of great flexibility in terms of accessible composition ranges due to the number of crystallographic sites available for chemical substitution. The ferroic properties of interest are coupled with strain, which will be important in the context of stability, switching dynamics and thin film properties. Coupling of strain with the ferroelectric order parameter gives rise to changes in elastic properties, and these have been investigated for a ceramic sample of $Ba_6GaNb_9O_{30}$ (BGNO) by resonant ultrasound spectroscopy. Room temperature values of the shear and bulk moduli for BGNO are rather higher than for TTBs with related composition which are orthorhombic at room temperature, consistent with suppression of the ferroelectric transition. Instead, a broad, rounded minimum in the shear modulus measured at $\sim$1 MHz is accompanied by a broad rounded maximum in acoustic loss near 115 K and signifies relaxor freezing behaviour. Elastic softening with falling temperature from room temperature, ahead of the freezing interval, is attributed to the development of dynamical polar nanoregions (PNRs), whilst the nonlinear stiffening below $\sim$115 K is consistent with a spectrum of relaxation times for freezing of the PNR microstructure.

✉ Andrei Rotaru
andrei.rotaru@inflpr.ro

[1] Faculty of Sciences, University of Craiova, Str. A.I. Cuza, Nr. 13, Craiova, Jud. Dolj, Romania

[2] Department of Earth Sciences, University of Cambridge, Downing Street, Cambridge CB2 3EQ, UK

[3] Laser Department, INFLPR – National Institute for Laser, Plasma and Radiation Physics, Bvd. Atomistilor, Nr. 409, Măgurele (Ilfov), Bucharest, Romania

Keywords Bulk modulus · Ceramics · Elastic properties · Phase transitions · Polar nanoregions (PNRs) · Relaxor dielectrics · Resonant ultrasound spectroscopy (RUS) · Shear modulus · Tetragonal tungsten bronzes (TTBs)

Introduction

The high permittivity of polar dielectrics such as piezoelectrics or ferroelectrics has made these materials particularly useful in electronic devices, with broad application in devices such as capacitors and resonators [1]. To date, much of the search for such new materials has largely centred on perovskite-based (ABO_3) materials, but these systems have a number of commonly encountered drawbacks. Firstly, many of the best performing materials require the presence of lead (Pb) in the structure, with associated difficulties associated with its toxicity in manufacturing, use and disposal. Secondly, many of these materials exhibit poor dielectric properties (leakage between active ions) resulting in the inability to sustain an electric field sufficient for hysteretic switching. Thirdly, for multiferroic perovskite systems, exhibiting both electrical and magnetic order simultaneously, the temperature of magnetic ordering is often below ambient temperature, or even when this is not the case, the coupling between magnetic and electrical order at room temperature is often very weak [2]. Nevertheless, some of these problems have been ameliorated either by finding new lead-free materials such as $K_{1-x}Na_xNbO_3$ (piezoelectric) [3], doping by single site substitutions, or by solid solution formation between ferroelectric, antiferro- and ferromagnetic perovskites including $BiFeO_3$–$PbTiO_3$ and $BiFeO_3$–$BaTiO_3$ [4].

Recently, the tetragonal tungsten bronze (TTB) class of materials—a structure closely related to perovskites, has

gathered the attention of the research community. The TTB structure: $(A1)_2(A2)_4(C)_4(B1)_2(B2)_8O_{30}$, due to the presence of crystallographically nonequivalent A- and B-sites and an extra C-site, provides supplementary degrees of freedom for manipulation of the structure, huge compositional flexibility allowing the insertion of various metals into the five different TTB sites [5], nevertheless offering the possibility of fine-tuning both electrical and magnetic behaviour [6, 7]. The TTB structure consists of a network of corner sharing BO_6 octahedra formed around the perovskitic A1 site that creates further two types of channels: pentagonal A2 channels (which can be occupied by alkali, alkaline earth and rare earth cations) and smaller triangular C channels (mostly vacant, they can be filled/just partially filled by small low-charged cations like Li^+—e.g., $K_6Li_4Nb_{10}O_{30}$). These materials, known to exhibit diverse properties as a result of compositional flexibility and by a higher probability for cation ordering, may offer better ways of attaining room-temperature ferroelectricity and (anti)ferromagnetism, multiferroic behaviour and eventually magnetoelectric coupling [2, 8]. Whilst ferroelectric TTBs (including $Ba_2NaNb_5O_{15}$ [9–11] and $(Ba,Sr)Nb_2O_6$ [12–14]) were widely investigated during the 1960s and 1970s, our understanding of manipulating this structure type is still poor, with the research surprisingly limited compared to that in perovskites [5]. Early attempts focused on tungsten bronzes of nominal composition $A_6B_{10}O_{30}$ (mainly compositions where the C-sites are vacant). A particular interest was developed regarding the Nb-based TTBs [15–17] due to their enhanced ferroelectric properties over other analogues such as Ta [18, 19]. In the search for novel multiferroic and magnetoelectric materials, the effect of the A-site size in a family of unfilled ferroelectric TTBs $Ba_4RE_{0.67}Nb_{10}O_{30}$ (RE = La, Nd, Sm, Gd, Dy, Y) [6] and of the A-site strain on dipole stability in fully filled TTBs family $A_6GaNb_9O_{30}$ (A = Ba, Sr, Ca) [7, 20] was studied. In addition to their ferroelectric and/or magnetic behaviour, the majority of TTBs reported in the literature exhibit relaxor properties [21–26]. Most TTBs that have been investigated to date are also lead-free materials [21, 22, 27].

In recent years, the research dedicated to novel TTB ferroelectric and ferroelectric-related (i.e., relaxors) materials has undergone a revival, with $Ba_6FeNb_9O_{30}$ (BFNO) as a starting point; many related compositions [28–31] or solid solutions, usually containing lanthanides [32–36], were studied. Arnold and Morrison [5], and subsequently Liu et al. [37], showed that these compounds display relaxor-type behaviour [38–40], with the peak maxima in the dielectric permittivity occurring in the temperature range 130–150 K. Earlier data indicated that BFNO is not electrically homogeneous [34], with oxygen vacancy gradients due to the variable oxidation state of Fe (Fe^{3+}/Fe^{2+}), as both low-temperature dielectric spectroscopy (DS) and high-temperature impedance spectroscopy (IS) data revealed a higher number of electroactive regions than expected [5]. In order to avoid these additional complications whilst studying such materials, the replacement of Fe^{3+} with Ga^{3+} (similar in size) and other trivalent species like Sc^{3+} and In^{3+} was proposed [5]. In previous research, temperature-dependent powder neutron diffraction (TDPND) and microstructural characterisation by scanning electron microscopy (SEM) confirmed the nature of the phases formed and contributed to their crystallographic identification [41]. Moreover, the origin of the polar response and the nature of the relaxor behaviour were established by combining the results of the structural investigations with the dielectric properties inspected by immittance spectroscopy (IS) [7, 41], whilst the dynamics of dielectric relaxation of dipoles was understood by fitting the dielectric data (permittivity and loss) with the Vogel–Fulcher (VF) and the universal dielectric response (UDR) models [42].

The bulk ferroelectric and magnetic properties of interest in the context of potential device applications involve changes in structure or electronic state which are almost invariably accompanied by lattice distortions that can be characterised as strain. Anisotropic strains are likely to improve the capacity of a material to retain an imposed dipole orientation, but repeated switching is then likely to result in mechanical failure. In thin film applications, the influence of strain imposed by mismatch of lattice parameters with the substrate is also a major consideration in engineering desired properties, in terms of both the stability of induced dipoles and the dynamics of their switching. If there is a change in strain state, it inevitably follows that there is a change in elastic properties which might be fundamental to making a particular ferroelectric distortion stable (for large strains), or simply an associated consequence (small strains). Formally there is coupling between strain, e, and the ferroelectric (or magnetic) order parameter, Q, that can take the form λeQ, λeQ^2, λe^2Q^2, λe^2Q, etc., depending on strict symmetry rules, where the coupling coefficient, λ, represents the strength of this coupling [43]. Such coupling results in the interaction length of the order parameter being determined by the strain field, which is typically long ranging. In this case, the overall thermodynamic behaviour is likely to follow the precepts of mean field theory. Considered from this perspective, it is understandable why investigation of both the strains themselves and of the changes in elastic properties which accompany them can provide insights into the static and dynamic properties of ferroic and multiferroic materials [44].

In this paper, we present results for the elastic properties of the relaxor dielectric $Ba_6GaNb_9O_{30}$ (BGNO) ceramic

material, with the TTB structure, obtained using resonant ultrasound spectroscopy (RUS), and relate the temperature-dependent elastic behaviour to the structural phase transitions previously observed by low-temperature dielectric spectroscopy [5, 6]. Resonant ultrasound spectroscopy is a powerful thermal analysis technique—belonging to the mechanical subgroup together with the thermomechanical analysis (TMA) and dynamical mechanical analysis (DMA)—dedicated to the study of fundamental properties involving elasticity [44–49]. When mechanically excited, solid bodies exhibit natural frequencies (depending on the elastic moduli, size, mass and shape) at which they vibrate [47, 48]. By exploiting this property of solids, the RUS technique determines the elastic tensor (elastic constants) of the material as a function of temperature from the resonance frequencies of the freely vibrating sample [49] and is an effective tool to monitor variations associated with structural transitions mainly due to its direct nature of sensing the structure [45]. Recently, the elastic properties of several relaxor systems were investigated by the RUS technique [50–53], and it has been applied by Pandey et al. [54–57] to investigate relaxor behaviour of Ca- and Sr-doped $Ba_5Nb_{10}O_{30}$ TTBs. We report new experimental determinations of the bulk and shear moduli of polycrystalline ceramic BGNO at room temperature, including corrections for the effects of for porosity [58], and compare them with values obtained for single-crystal TTB compounds with similar structures [59]. Variations of the shear modulus and of acoustic loss as a function of temperature through interval 10–300 K are interpreted in terms of the dynamics and freezing behaviour of PNRs.

Experimental

$Ba_6GaNb_9O_{30}$ (BGNO) powder was synthesised by standard solid-state techniques. Stoichiometric ratios of dried $BaCO_3$, Nb_2O_5 and Ga_2O_3 (all Aldrich, 99+ %) were ball-milled under ethanol until homogenised, 5 min at 400 rpm, using a Fritsch Pulverisette 7 system with agate mortar and balls. The produced powder was placed on platinum foil, in alumina boats and fired in a muffle furnace (static air atmosphere) straight to 600 °C. It was heated from 600 to 1000 °C, left to decarbonate for 1 h and then fired for 12 h at 1250 °C. Afterwards, it was quenched to room temperature, reground and heated back at 1250 °C for 12 h more in alumina boats (placed on platinum foil) inside the same muffle furnace. Finally, a third thermal process was carried out for 12 h at 1300 °C; the boats containing the previously ball-milled powders were placed in the middle of a tube furnace, and radiation shields were used at both ends of the alumina tube to maintain a more stable temperature (the conditions inside the tube were still at atmospheric pressure). For obtaining $Ba_6GaNb_9O_{30}$ pellets, the powders were pressed in a 10-mm-diameter uniaxial stainless steel die to 1 tonne, producing a pressure of around 200 MPa followed by sintering in a tube furnace for 12 h at 1250 °C (heating and cooling rates were of 10 K min^{-1}). Phase formation was confirmed by powder X-ray diffraction and temperature-dependent powder neutron diffraction; at room temperature, diffraction data were refined with the centrosymmetric tetragonal space group *P4/mbm* [5, 41, 42].

Rectangular parallelepipeds within millimetre range of the edge lengths were cut from the pellets described above using a fine annular diamond saw lubricated with paraffin. The pellets were initially glued onto a flat glass surface with Crystalbond glue (with the softening temperature: 120–130 °C), and the cuts were made perpendicular to the glued surface whilst rotating by 90 several times until obtaining complete rectangular parallelepipeds. The glue was removed by heating and washing with acetone. The parallelepipeds were subsequently polished using a stable vertical steel lapping jig, fine polishing paper and a bed of acetone to remove cracks and until achieving optical quality. A parallelepiped-shaped sample of $m = 0.1991$ mg and $\rho_r = 94.43$ %, with dimensions $2.346 \times 3.241 \times 4.757$ mm^3, was employed for the resonant ultrasound spectroscopy measurements.

The RUS spectra of the BGNO sample were first collected at room temperature (RT) by exciting the sample at frequencies between 0.1 and 1.2 MHz (65,000 data points per spectrum). The parallelepiped was remounted in different orientations between the two piezoelectric transducers (across corners, edges, faces) for successive spectra so as to ensure that all resonances are observed at least two times. The spectra were analysed offline using the software package Igor Pro (WaveMetrics), whilst the stack of spectra were plotted here as amplitude versus frequency in Origin7.5 software. Bulk (K) and shear (G) moduli were determined by matching—nonlinear least-squares refinement—the observed resonance frequencies with the calculated resonance frequencies using the RPR fitting procedure [49]. The obtained values of the elastic moduli were corrected for porosity following the correction equations proposed by Ledbetter et al. [58] and compared with those obtained for two single-crystal TTB compounds with similar structure [59]; the two single-crystal TTBs $Ba_{2.8}Sr_{1.2}Na_2Nb_{10}O_{30}$ and $Ba_{1.2}Sr_{2.8}Na_2Nb_{10}O_{30}$ used for this comparison belong to the $(Ba_{1-x}Sr_x)_4Na_2Nb_{10}O_{30}$ class and were investigated by means of ultrasonic measurements, which provided the entire set of characteristic elastic constants [59], whilst we have calculated further their isotropic equivalent elastic moduli by employing these previously reported data and the relevant equations facilitating the conversion to a polycrystalline ensemble from the moduli in the original orthorhombic symmetry.

Low-temperature RUS measurements were carried out with the sample resting lightly between the transducers across a pair of faces. Again the sample was excited at frequencies between 0.1 and 1.2 MHz with 65,000 data points per spectrum. The head assembly was held vertically in a helium-flow cryostat in an atmosphere of few millibars of He to facilitate heat transfer, as described previously by McKnight et al. [60, 61]. Sequences of spectra were collected during cooling and heating between $\sim$300 and $\sim$10 K, and a period of 20 min was allowed for thermal equilibration at each temperature before data collection. The frequency, f_p, and width, Δf, for selected resonance peaks were obtained by fitting with an asymmetric Lorentzian function. The elastic constants which determine the resonant behaviour of an individual mode scale with f_p^2 for that mode, and the acoustic loss is given in terms of the inverse mechanical quality factor, Q^{-1}, which can be expressed as $\Delta f/f_p$. Most mechanical resonances of a small object are determined predominantly by shearing motions so that the temperature dependence of f_p^2 provides a good representation of the temperature dependence of the shear modulus.

Results and discussion

Usually, the most common technique employed to investigate ferroelectric and relaxor properties of bulk ceramics is dielectric spectroscopy. However, as stated in the introductory part of this paper, mechanical spectroscopy is a useful tool which completes the general understanding of materials' structure, the structural evolution and structure–property relationships, by revealing the elastic properties of materials. Generally, elastic constants change due to the high sensitivity of the material to induced strain, regardless of the excitation applied: mechanical, thermal, electric, magnetic, etc. In our particular case, differences between the results obtained from dielectric and mechanical spectroscopies might be due to the relatively strong and short-ranging interactions between electric dipoles on one side, and due to the weaker but long-ranging elastic strain fields on the other [46]. In a tetragonal structure, for example, there is no strain across twin walls between 180° domains which are nonetheless ferroelectric and thus respond only to an applied electric field, whilst the twin walls between 90° domains are both ferroelectric and ferroelastic, yielding an extrinsic response to a stress field; as a result, the dielectric loss and the acoustic loss will in general be different [46]. It is clear that the advantages of using a mechanical spectroscopy technique like RUS lie in the interesting attribute strain coupling phenomena to all structural changes that may be otherwise found from dielectric spectroscopy, magnetic studies, calorimetry, X-ray and neutron diffraction, etc. In the case of RUS, mechanical energy losses are not affected by bonding agents, transducers and issues such as the scattering of laser beams is not an issue and true sample dissipation may be directly observed (RUS resonances are standing waves) [62].

Elastic properties at room temperature

An elastic modulus describes how resistant a material is to strain when subjected to an applied stress; in reality, materials are stiffer in some directions compared to others, resulting in the existence of several oriented elastic moduli according to Hooke's law:

$$\sigma_i = c_{ik} \cdot e_k \tag{1}$$

where σ_i is the second-rank stress tensor, e_k is the second-rank strain tensor, and c_{ik} is the fourth-rank elastic constant tensor. The symmetry of the material determines the form of the elastic constant tensor with a maximum of 21 independent elastic constants for a triclinic crystal and 3 for a cubic crystal [63]. The elastic behaviour of a polycrystalline material is usually described by its bulk modulus, K (resistance to uniform compression), and its shear modulus, G (resistance to shear stress). In a polycrystalline material, each individual grain is usually anisotropic, but if their orientation is random, the bulk sample will be isotropic. In this case, the elastic moduli can be expressed either in terms of the bulk and shear moduli or in terms of two elastic constants, c_{11} and c_{44}, which are related by

$$K = \frac{1}{3} \cdot (c_{11} + 2 \cdot c_{12}) \tag{2}$$

$$G = c_{44} = \frac{1}{2} \cdot (c_{11} - c_{12}) \tag{3}$$

In order to refine K and G values for polycrystalline $Ba_6GaNb_9O_{30}$ (BGNO) from the measured resonance frequencies, it was necessary to start with trial values taken from the literature. Data from ferroelectric single crystals of $(Ba_{1-x}Sr_x)_4Na_2Nb_{10}O_{30}$ ($x = 0.3$ and 0.7) solid solutions which were previously investigated by means of ultrasonic measurements to provide the entire set of characteristic elastic constants [59] were utilised for this purpose here. Although the end members of this family are known to have orthorhombic (in the Sr-rich compound) and tetragonal (in the Ba-rich compound) symmetry at room temperature, for the two single-crystal compounds investigated in Ref. [59] it is practically impossible to establish the symmetry for certain, and a morphotropic phase boundary has been proposed for $x = 0.6$ [59, 64]. However, the discussion regarding the elastic properties was carried

out, further assuming orthorhombic symmetry and 17 independent constants: 9 elastic, 5 piezoelectric and 3 dielectric [59].

For calculating the elastic moduli of $Ba_{2.8}Sr_{1.2}Na_2Nb_{10}O_{30}$ and $Ba_{1.2}Sr_{2.8}Na_2Nb_{10}O_{30}$ (Table 1), we have employed the previously reported elastic constants ("Appendix") [59] and made use of the equations specific to the orthorhombic symmetry (Eqs. 4–10) [65]; for an orthorhombic crystal, the single-crystal elastic constants are c_{11}, c_{22} c_{33}, c_{44}, c_{55}, c_{66}, c_{12}, c_{13}, c_{23}. Since the effective bulk and shear moduli of a polycrystalline material cannot be precisely calculated from its individual single-crystal grains' elastic constants, a variety of averaging techniques have been proposed [66–68]. The conventional average value lies between two limits, the lower one, named the Reuss limit, is calculated assuming that the stress is uniform—Eqs. 6 and 7 [66], and the higher one, named the Voigt limit, is calculated assuming that the strain is uniform—Eqs. 4 and 5 [67]. However, it is impossible to have uniform stress or strain in real polycrystalline materials; therefore, the most suitable approximation is their arithmetic average, known as the Voigt–Reuss–Hill average—Eqs. 9–10 [69].

$$K_V = \frac{1}{9}\cdot[c_{11}+c_{22}+c_{33}+2\cdot(c_{12}+c_{13}+c_{23})] \tag{4}$$

$$G_V = \frac{1}{15}\cdot[c_{11}+c_{22}+c_{33}+3\cdot(c_{44}+c_{55}+c_{66}) -(c_{12}+c_{13}+c_{23})] \tag{5}$$

$$K_R = \Delta\cdot[c_{11}\cdot(c_{22}+c_{33}-2\cdot c_{23})+c_{22}\cdot(c_{33}-2\cdot c_{13}) -2\cdot c_{33}\cdot c_{12}+c_{12}\cdot(2\cdot c_{33}-c_{12})+c_{13} \cdot(2\cdot c_{12}-c_{13})+c_{23}\cdot(2\cdot c_{13}-c_{23})]^{-1} \tag{6}$$

$$G_R = 15\cdot\left\{4\cdot[c_{11}\cdot(c_{22}+c_{33}+c_{23})+c_{22}\cdot(c_{33}+c_{13}) +c_{33}\cdot c_{12}-c_{12}\cdot(c_{12}+c_{23})-c_{13}(c_{13}+c_{12}) -c_{23}\cdot(c_{23}+c_{13})]/\Delta+3\cdot\left(\frac{1}{c_{44}}+\frac{1}{c_{55}}+\frac{1}{c_{66}}\right)\right\}^{-1} \tag{7}$$

$$\Delta = c_{13}\cdot(c_{12}\cdot c_{23}-c_{13}\cdot c_{22})+c_{23}\cdot(c_{12}\cdot c_{13}-c_{23}\cdot c_{11}) +c_{33}\cdot\left(c_{11}\cdot c_{22}-c_{12}^2\right) \tag{8}$$

$$K_{VRHavrg} = \frac{K_V+K_R}{2} \tag{9}$$

$$G_{VRHavrg} = \frac{G_V+G_R}{2} \tag{10}$$

For $Ba_{1.2}Sr_{2.8}Na_2Nb_{10}O_{30}$, the differences between both K and G values corresponding to Voigt and Reuss limits are large (171.44 vs. 23.67 GPa for K and 50.99 vs. 37.87 GPa for G), giving low average values of $K_{VRHavrg}$ and $G_{VRHavrg}$ when compared to those of $Ba_{2.8}Sr_{1.2}Na_2Nb_{10}O_{30}$ (Table 1). Such large differences between samples with similar chemistry and structure are most likely due to the influence of strain coupling at a phase transition which must be nearby in temperature-composition space.

In order to understand the variations in the elastic behaviour of BGNO with temperature, the first step is to investigate and understand its elastic properties at room temperature. In this regard, we have used the RUS technique to measure the normal frequencies of vibration in a range of frequencies between 0.1 and 1.2 MHz (Fig. 1) as described above. The normal frequencies of vibration depend on the crystallographic structural symmetry, macroscopic sample symmetry and characteristics (shape, dimensions and density). As is the case in any real material, the stress and the displacement are somewhat out of phase, thus the magnitude of the measured displacement having two components (real and imaginary) [49]. The two components—"in phase" and "quadrature" of the signal are detected and converted into amplitude (in V) according to Eq. 11; the output spectrum of the RUS experiment consists of a series of peaks which occur at the resonance frequencies of the natural mechanical resonances of the BGNO sample (Fig. 1a).

$$\text{Amplitude} = \sqrt{\text{inphase}^2+\text{quadrature}^2} \tag{11}$$

By supporting the BGNO sample in opposite corners between the piezoelectric transducers, the loading is reduced on the sample, elasticity is maximal compared to the case of edges and faces, and therefore the coupling to all normal vibrational modes led to the impossibility of losing resonance [45]. Furthermore, other mounting orientations of the BGNO parallelepiped—edges and faces—were utilised several times on different parts of the sample in order to be sure of a sufficiently complete data

Table 1 Bulk and shear elastic moduli of $(Ba_{1-x}Sr_x)_4Na_2Nb_{10}O_{30}$ ($x = 0.3$ and 0.7) solid solutions at room temperature, according to Voigt limit, Reuss limit and Voigt–Reuss–Hill average

Compound	Elastic moduli					
	K_V/GPa	G_V/GPa	K_R/GPa	G_R/GPa	$K_{VRHavrg}$/GPa	$G_{VRHavrg}$/GPa
$Ba_{2.8}Sr_{1.2}Na_2Nb_{10}O_{30}$	127.11	66.87	89.67	65.37	108.39	66.12
$Ba_{1.2}Sr_{2.8}Na_2Nb_{10}O_{30}$	171.44	50.99	23.67	37.87	97.56	37.87

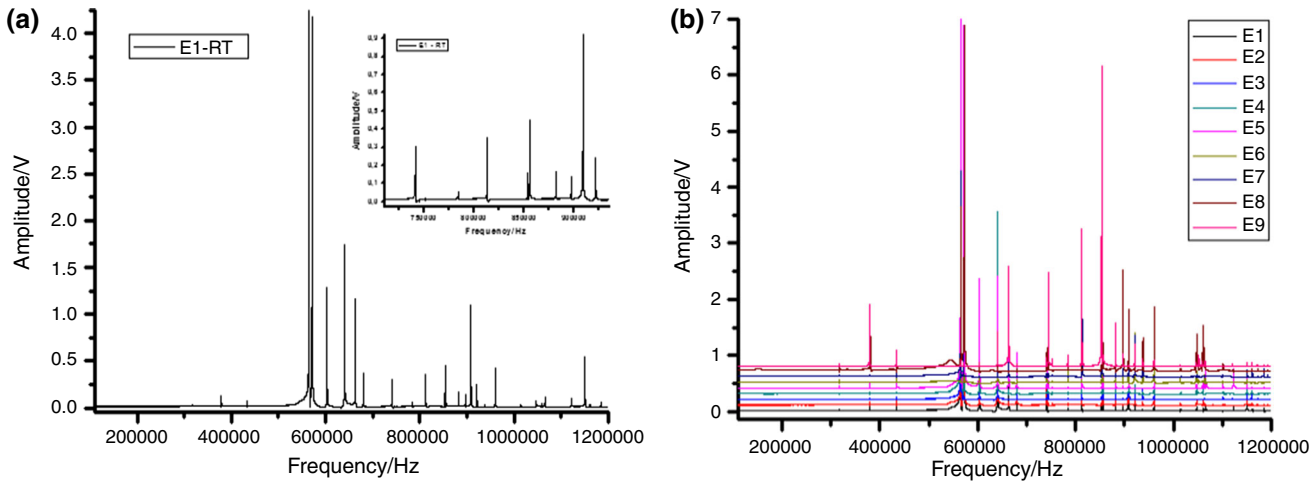

Fig. 1 RUS spectra collected between 0.1 and 1.2 MHz at room temperature for $Ba_6GaNb_9O_{30}$ (BGNO) in **a** one corner orientation and **b** several orientations comprising corners, edges and faces (displacement step: 0.1)

collection, giving the presence of all resonance frequency peaks, preferably with optimal shapes and amplitudes, which are mainly dependent on the mechanical coupling between the samples than the transducers (Fig. 1b). All in all, the resonant ultrasound spectra of BGNO dense ceramic contain uniformly nondegenerate resonances, since rectangular parallelepipeds were used, and all modes were observed individually.

The absolute values of the amplitudes are variable for every measurement, highly depending on the mechanical coupling, orientation and position of the parallelepiped sample relative to the transducers; however, the peak frequencies [39] and their widths at half maximum are characteristic to the BGNO sample, offering the possibility to determine the elastic and anelastic properties, if properly measured. The output of a calculation of the elastic moduli from RPR is shown in Table 2.

Observation of the first few peaks at low frequencies, and in particular the first one, is of key importance for the fitting procedure and the calculation of the elastic constants and elastic moduli; specifically, the first resonance peak has a 100 % shear contribution (Table 2), and thus an error in this peak can lead to detrimental shifts throughout the pattern. The elastic constants (c_{11} and c_{44}) of the sample and thus the elastic moduli (K and G) of polycrystalline BGNO ceramic were determined by the solution of a combined problem, using the method known as rectangular parallelepiped resonance (RPR) [70, 71] implemented in the RPR programme. This combined problem involves on one side a "forward" problem consisting of the calculation of the expected resonance frequencies from inputting data such as the dimensions, mass, density and guesses of elastic constants [49] and on the other side a "inverse" problem consisting in calculating the elastic constants from the experimental resonance frequencies of the eigenmodes [45]. The Lagrangian minimisation of the free energy function was used by applying the Rayleigh–Ritz approximation method for solving the "forward" problem [72], and further the Levenberg–Marquardt algorithm was used to carry out the least-squares fitting procedure between the guess elastic constants and the calculated elastic constant for solving the "inverse" problem and convergence [49]. Moreover, if a peak is not observed, the RPR programme gives certain signals that it is missing and thus its presence may be included in the input file either through direct observation on the room-temperature measurements, or if, for example, one peak out of more than 20 is not observed in the measurements, it can be omitted and left as an unrefined dummy value. This was not required for this sample, but is standard practice when the specific coupling has not yielded every peak, or where accidental degeneracy obscures one of a pair of peaks, for example.

One of the most important issues when determining the elastic constants/elastic moduli is represented by the starting guess values; in order not to reach a false minimum during the fitting process, the guess values of elastic constants/elastic moduli assumed for BGNO were chosen from those previously determined and belonging to $(Ba_{1-x}Sr_x)_4Na_2Nb_{10}O_{30}$ class, more exactly to the Ba-rich member, $Ba_{2.8}Sr_{1.2}Na_2Nb_{10}O_{30}$ (Table 1). The guess values for the bulk and shear moduli of BGNO were, as mentioned above, $K_{guess} = K_{VRHavrg} = 108.39$ GPa and $G_{guess} = G_{VRHavrg} = 66.12$ GPa. These guess values contributed to the rapid convergence of the calculation of the expected resonance frequencies with small errors (Table 2). After the refinement of the eigenmode frequencies in the RPR programme, the calculated values of the elastic moduli for the BGNO sample were $K_{ex} = 118.7(6)$ GPa and

Table 2 Results of the RPR combined problem for BGNO: $f_{experimental}$ versus $f_{calculated}$ and contribution of K versus G

n	$f_{experimental}$/MHz	$f_{calculated}$/MHz	Error%	K contribution/%	G contribution/%
1	0.317264	0.316601	−0.21	0	100
2	0.379124	0.378884	−0.06	21	79
3	0.433634	0.432928	−0.16	22	78
4	0.564551	0.564196	−0.06	4	96
5	0.571280	0.570026	−0.22	15	85
6	0.603219	0.603510	0.05	6	94
7	0.640412	0.640188	−0.03	6	94
8	0.663299	0.661657	−0.25	31	69
9	0.679701	0.678914	−0.12	1	99
10	0.741074	0.740590	−0.07	23	77
11	0.744577	0.743189	−0.19	16	84
12	0.751383	0.749973	−0.19	16	84
13	0.783987	0.783600	−0.05	2	98
14	0.812832	0.812939	0.01	9	91
15	0.853242	0.852523	−0.08	19	81
16	0.855377	0.854068	−0.15	4	96
17	0.881732	0.880093	−0.19	5	95
18	0.897118	0.896251	−0.10	8	92
19	0.908511	0.909445	0.10	13	87
20	0.920765	0.920003	−0.08	13	87
21	0.937236	0.940008	0.30	9	91
22	0.960226	0.960422	0.02	14	86
23	1.014775	1.016764	0.20	2	98
24	1.046066	1.045456	−0.06	7	93
25	1.047637	1.049133	0.14	31	69
26	1.048593	1.051636	0.29	0	100
27	1.052019	1.057208	0.49	8	92
28	1.057828	1.060486	0.25	27	73
29	1.060844	1.060830	0.00	21	79
30	1.063554	1.061987	−0.15	22	78
31	1.066700	1.067430	0.07	18	82
32	1.101404	1.108516	0.65	19	81
33	1.122199	1.124902	0.24	29	71
34	1.150630	1.151159	0.05	11	89
35	1.159716	1.158803	−0.08	10	90
36	1.161187	1.160093	−0.09	11	89
37	1.171896	1.169337	−0.22	29	71
38	1.185389	1.185586	0.02	10	90
39	1.191960	1.190993	−0.08	11	89

$G_{ex} = 67.96(4)$ GPa (Table 3). Since the BGNO polycrystalline ceramic sample used has a density which is 94.43 % of the theoretical density calculated from lattice parameters, it is not possible to directly compare the experimental values of the bulk and shear moduli to those of fully dense single crystals. Ledbetter et al. [58] have proposed a model that takes into account pores and voids and corrects the experimental elastic moduli values by assuming randomly distributed spherical voids with no elastic resistance to dilatation and shear. The intrinsic bulk and shear moduli of the material for an ideal 100 % dense ceramic, K_m and G_m, are calculated by means of Eqs. 12–16, where "c" stands for the void fraction [58].

Table 3 Bulk and shear elastic moduli of $Ba_6GaNb_9O_{30}$ polycrystalline ceramic before and after correcting for porosity, in comparison with single-crystal $(Ba_{1-x}Sr_x)_4Na_2Nb_{10}O_{30}$ ($x = 0.3$ and 0.7) solid solutions

Compound	K_{ex}/GPa	G_{ex}/GPa	RMSD%	ρ_r/%	K_m/GPa	G_m/GPa
$Ba_6GaNb_9O_{30}$	118.7(6)	67.96(4)	0.1953	94.43	135.06	75.75
$Ba_{2.8}Sr_{1.2}Na_2Nb_{10}O_{30}$	–	–	–	N/A	108.39	66.12
$Ba_{1.2}Sr_{2.8}Na_2Nb_{10}O_{30}$	–	–	–	N/A	97.56	37.87

$$K_m = \frac{4 \cdot G_m \cdot K_{ex}}{4 \cdot (1-c) \cdot G_m - 3 \cdot c \cdot K_{ex}} \quad (12)$$

$$G_m = \frac{1}{2 \cdot A_1}\left[-A_2 + \left(A_2^2 - 4 \cdot A_1 \cdot A_3\right)^{1/2}\right] \quad (13)$$

$$A_1 = \frac{8}{3}(1-c) \quad (14)$$

$$A_2 = (3 - 2 \cdot c) \cdot K_{ex} - \left(\frac{8}{3} + 4 \cdot c\right) + G_{ex} \quad (15)$$

$$A_3 = -3 \cdot (1+c) \cdot K_{ex} \cdot G_{ex} \quad (16)$$

After applying the correction for porosity to the experimental moduli values, the intrinsic bulk and shear moduli of the BGNO ceramic were obtained: $K_m = 135.06$ GPa and $G_m = 75.75$ GPa (Table 3).

Both the bulk and shear intrinsic moduli values of BGNO are higher than those of $Ba_{2.8}Sr_{1.2}Na_2Nb_{10}O_{30}$ and $Ba_{1.2}Sr_{2.8}Na_2Nb_{10}O_{30}$ ($K_m = 108.39$ GPa and $G_m = 66.12$ GPa, respectively, $K_m = 97.56$ GPa and $G_m = 37.87$ GPa), indicating a tendency of increasing material resistance to both uniform compression and shear stress with increasing Ba^{2+} content. This is likely due to the bigger cation size on the A-site within the TTB structure which will lower the temperature for a tetragonal—orthorhombic transition. In other words, BGNO at room temperature has the relatively stiff elastic properties of the high-symmetry TTB structure, whilst the Sr phases probably show the effects of elastic softening associated with transformation to the orthorhombic structure.

Temperature-dependent elastic properties

The great interest in following changes in the elastic properties of materials with temperature variation derives from a need to understand the structural and thermodynamic behaviour of those materials, across phase transitions. During phase transitions, the elastic properties exhibit important anomalies, often in the form of elastic softening, with specific elastic moduli tending to zero in some classes of phase transition. Structural phase transitions can be related to elastic behaviour through the use of Landau theory [73], briefly defined as a "phenomenological description of the free energy across the transition as a function of temperature, in terms of the driving order parameter, the strains and the coupling between the order parameter and the strains" [45].

Resonance ultrasound spectroscopy (RUS) combines in a single experiment information regarding the elasticity, ferroic properties and microstructure dynamics [45]. The relatively recent approach of using RUS as a thermal analysis method for studying elastic properties associated with phase transitions allows the rapid and relatively simple collection of data the previously required more complicated experiments and complicated equations employed by conventional mechanical techniques. RUS spectra of BGNO were recorded first during cooling between RT and 180 K every 30 K and then from 165 K down to 5 K in 10 K steps. During heating, the RUS spectra were collected from 5 to 290 K in 5 K steps. These are shown in stacks with an offset of each spectrum up the y-axis in proportion to the temperature at which it was collected (Fig. 2a; blue = cooling sequence, red = heating sequence). In order to have a better resolution of the temperature evolution of the resonant frequencies, we have shown a restricted frequency range, 1.005–1.670 MHz, in Fig. 2b. In broad terms, the elastic behaviour with reducing temperature shows softening down to a local minimum at around 115 K followed by stiffening down to the lowest temperatures measured. This is indicative of some structural instability since normal thermal expansion would be expected to cause continuously increasing elastic stiffness with falling temperature. Broadening of the peaks below the temperature at which the resonances reach their lowest frequencies is indicative of strong acoustic dissipation accompanying the instability.

A quantitative description of the elastic behaviour may be obtained by calculating the square of the frequencies belonging to the resonance peaks at all temperatures, f_p^2, which scales linearly with the elastic modulus [49]; therefore, a direct and relatively simple indication on the variation of the elastic moduli, in particular the shear elastic moduli, may be obtained in a straightforward manner. Complementary information that can also be obtained involves the anelastic dissipation—represented by the so-called mechanical quality factor, Q, which often shows the microstructural transformations, in particular those which depend on domain switching and movement of the twin walls. The inverse of the mechanical quality factor, which actually stands for the acoustic dissipation within the sample, may be calculated using Eq. 17; where

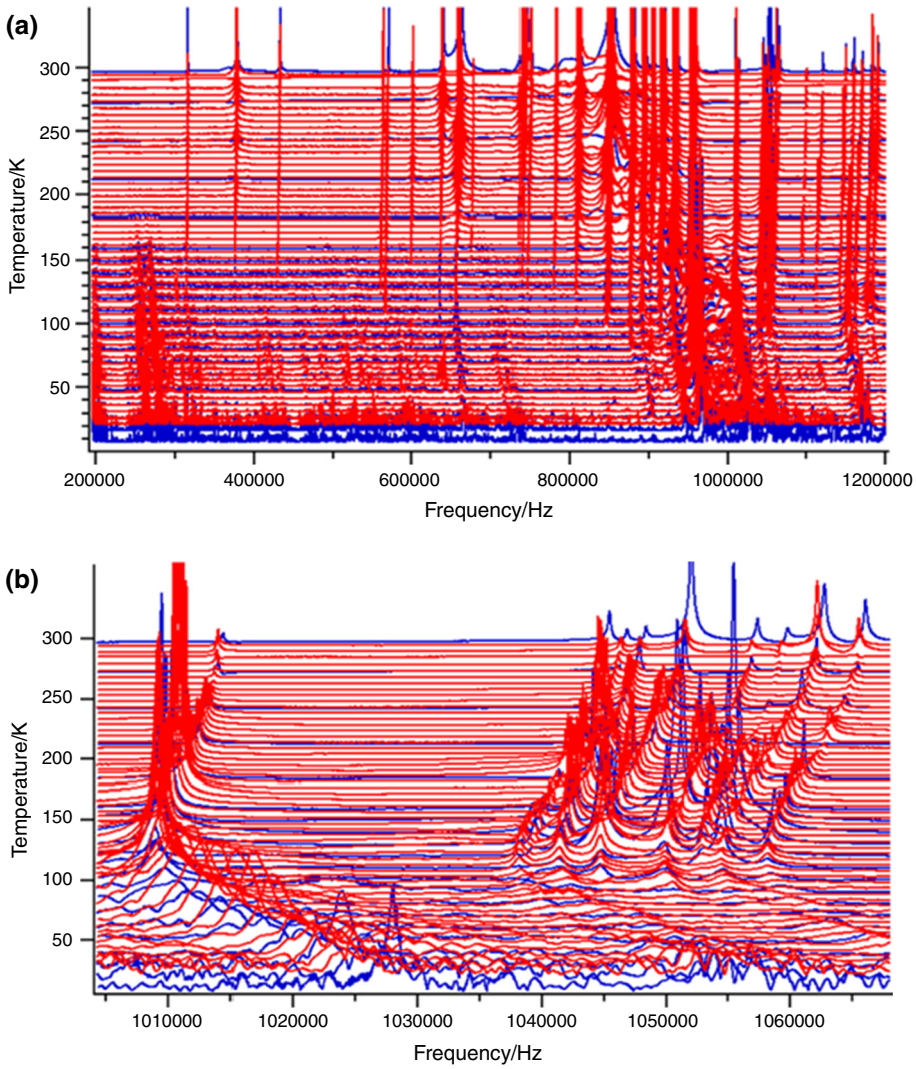

Fig. 2 RUS spectra at low temperatures between RT-5 K collected during cooling (*blue*) and subsequent heating (*red*) for $Ba_6GaNb_9O_{30}$ (BGNO) in the frequency region **a** 0.2–1.2 MHz and **b** 1.004–1.670 MHz. (Color figure online)

f_p is the peak frequency and Δf is the full width at half maximum of the peak.

$$Q^{-1} = \frac{\Delta f}{f_p} \tag{17}$$

A typical RUS resonance peak of BGNO sample is shown in Fig. 3, together with the Lorentzian asymmetric curve fit that gives the values of the assumed resonance frequency, f_p, and the width at half maximum of the peak, Δf.

In order to extract these values, the Igor Pro software was used for fitting each resonance peak by means of asymmetric Lorentzian function [74, 75], which implements the condition of fitting both sides of the peak with two different profiles (Eqs. 18 and 19).

$$A = w_0 + w_5 \cdot f + w_2/[(f - w_1)^2 + w_3]; \quad \text{if } f < w_1 \tag{18}$$

$$A = w_0 + w_5 \cdot f + w_4/[(f - w_1)^2 + (w_4 \cdot w_3/w_2)]; \quad \text{if } f \geq w_1 \tag{19}$$

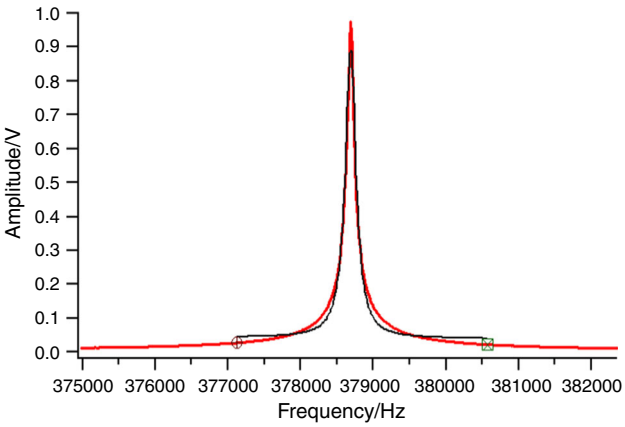

Fig. 3 Typical resonance peak from the RUS spectrum for $Ba_6GaNb_9O_{30}$ (BGNO) shown in Fig. 2 (*red line*); RUS peak fit by an asymmetric Lorentzian function shown in Eqs. 18 and 19 (*black curve*). (Color figure online)

where w_0 accounts for the background, w_1 corresponds to the peak frequency (f_p), w_2 relates to the left part of the curve, w_3 relates to the peak amplitude, w_4 relates to the right part of the curve, and w_5 accounts for the slope of the background. Input guesses for w_0, w_2, w_3, w_4 and w_5 were available from the literature [45], whilst w_1 was carefully chosen with the help of the cursor from Fig. 3-like plots. The results of the asymmetric Lorentzian fits of two sets of resonance peaks characteristic to BGNO ceramic (elastic parameters f_p^2 and Q^{-1}) were tabled and are further plotted in Fig. 4a, b (for a resonance peaks near 1 MHz in Fig. 4a during heating and cooling, and for two different peaks near 1 and 0.9 MHz during cooling in Fig. 4b) and compared with the dielectric spectroscopy (DS) data from Fig. 4c.

The softening of f_p^2 to a broad, rounded minimum without obvious hysteresis and subsequent stiffening are accompanied by a broad, asymmetric peak in Q^{-1} in both cases. The temperatures of the minima are the same within experimental uncertainty, and small differences between the f_p^2 values for the two peaks are due to slightly different contributions of K (2 vs. 9 %) and G (98 vs. 92 %) to each resonance mode (see Table 2 for peaks number 21 and 23). Below 90 K, a high level of acoustic loss, combined with decreased amplitude from the piezoelectric transducers, makes fitting of the peaks difficult, hence the larger scatter and occasional missing data, particularly for Q^{-1}. The imaginary part of dielectric spectra (dielectric loss) collected at 1 MHz is shown in Fig. 4c for comparison (see Ref. [6]).

This overall pattern is closely similar to that seen for the classic relaxor ferroelectric $Pb(Mg_{1/3}Nb_{2/3})O_3$ (PMN) described by Carpenter et al. [52] and is consistent with freezing of PNRs in a temperature interval below ~150 K. The onset of elastic softening for a relaxor ferroelectric appears to coincide with the Burns temperature (i.e., see Ref. [45]) which must be somewhat above room temperature for BGNO. The softening mechanism is likely to be due to coupling of acoustic modes with a central mode that is due to the dynamic PNRs. Increasing acoustic loss below ~150 K signifies slowing down of the PNR dynamics, and the peak at ~60 K signifies their freezing point ($\omega\tau = 1$, where ω is the measuring frequency and τ the relaxation time) at a measuring frequency of ~1 MHz. The evolution of the modulus at low temperature is required to undergo a flattening of the sort described by Varshni [76], and, as

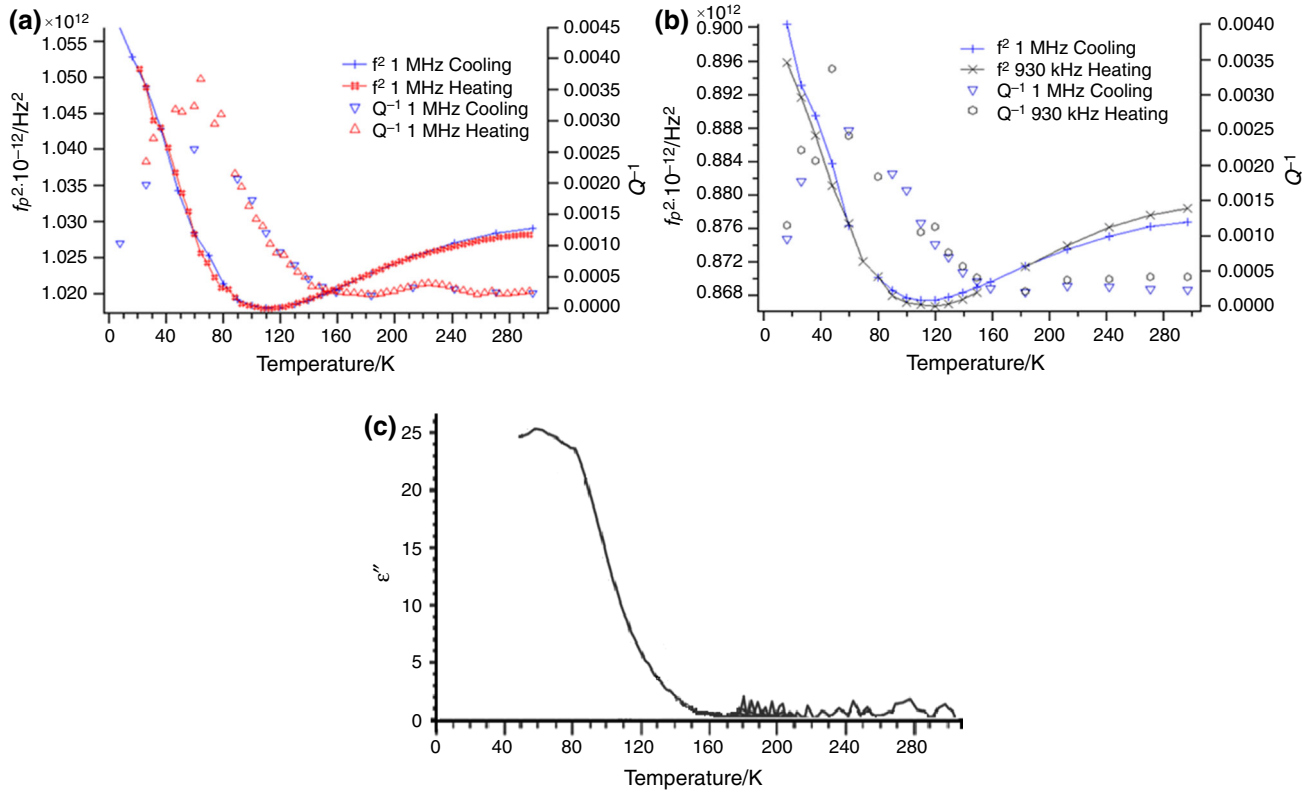

Fig. 4 Results from the analysis of RUS and DS spectra collected at low temperatures for $Ba_6GaNb_9O_{30}$ (BGNO). **a** f_p^2 and Q^{-1} from fitting of selected resonance peaks at the starting frequency (RT) of ~1 MHz, both during cooling (*blue*) and heating (*red*). **b** Comparison of f_p^2 and Q^{-1} from fitting of two resonance peaks at the room-temperature starting frequencies of ~1 MHz (*blue*) and ~930 kHz (*black*) (cooling only). **c** ε'' as function of temperature at 1 MHz, during cooling [6]. (Color figure online)

such, the continued stiffening at low temperatures is also anomalous. It can be explained if slowing down and/or freezing of defects [77] coupled with strains continues down to the lowest temperatures, indicating a widespread spectrum of relaxation times, which is a defining property of relaxor behaviour. A multitude of relaxational processes occurring and overlapping in the temperature range 50–100 K may explain the poor results obtained previously for extrapolating the freezing temperature of dipoles of BGNO from employing both universal dielectric response model (UDR) [78, 79] and the maximum of unit-cell tetragonality as a function of temperature (Figures 4d & 6a from Ref. [41]).

The elastic compliance, $1/f_p^2$, and the real part of the dielectric constant are compared in Fig. 5 and are also closely similar, as would be expected if essentially the same freezing process is being observed. Real and imaginary parts of the dielectric spectra reflect the freezing of PNRs from the perspective of changes in local dipoles, whilst the elastic compliance is a measure of the strength of strain coupling with these. There are small differences in the temperature of the maxima, however, which is a few degrees lower for the compliance (Fig. 5a) than for the dielectric constant (Fig. 5b). The same feature was seen in PMN and was explained in terms of the fact that the dielectric spectra detect freezing dynamics of 180° domain walls or boundaries between PNRs, whilst the elasticity data detect that of the 90° walls [52]. Additional small anomalies are definitely present in the dielectric data (at ~80 and ~60 K in Fig. 5b), which must be indicative of additional changes in dynamics and microstructure. These are perhaps evident in the compliance data (Fig. 5a), but the changes are barely, if at all, above the level of noise.

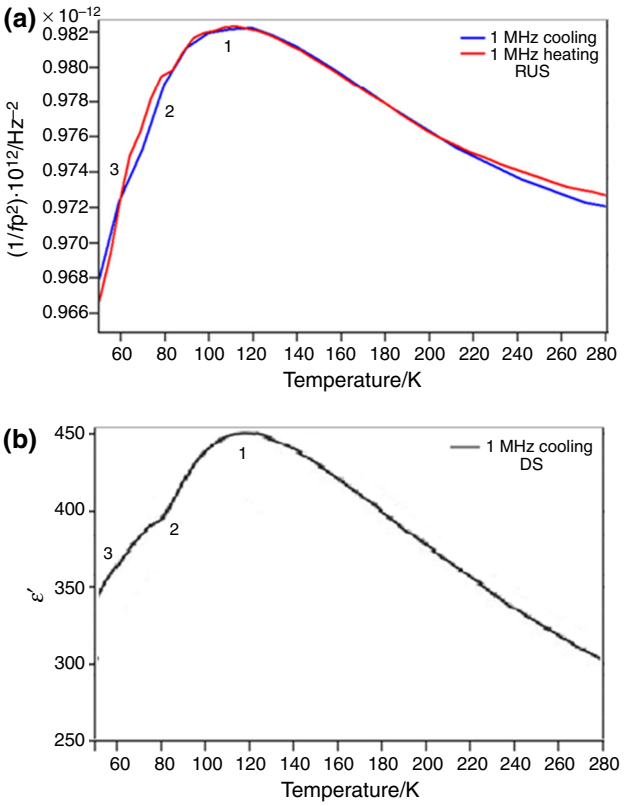

Fig. 5 **a** Results from the analysis of RUS and DS spectra collected at low temperatures for $Ba_6GaNb_9O_{30}$ (BGNO): **a** $1/f_p^2$ plot standing for the variation of elastic compliance from fitting of selected resonance peaks at the starting frequency (RT) of ~1 MHz, during both cooling (*blue*) and heating (*red*); **b** ε' as function of temperature at 1 MHz, during cooling only (*black*) [6]. (Color figure online)

Conclusions

The elastic and anelastic properties of $Ba_6GaNb_9O_{30}$ (BGNO) reveal a material which is significantly stiffer than related ferroelectric structures with nearby compositions, probably due to suppression of the ferroelectric transition. Instead, BGNO undergoes relaxor freezing in a temperature interval below ~150 K with anomalies in elastic properties which show that development of local ferroelectric dipoles also involves local strain variations; before the relaxor freezing, there is the formation of polar nanoregions (PNRs), which implies an elastic softening. A broad minimum in the shear modulus and a broad maximum in Q^{-1} reflect the wide spectrum of relaxation times which is believed to be at the heart of relaxor behaviour, and freezing of some parts of the PNR microstructure appears to extend down to the lowest temperatures. The sensitivity to composition could be exploited in the engineering of relaxor properties for device applications, and the significance of strain coupling is that these properties could also be engineered by the choice of strain imposed from a substrate.

Acknowledgements This work was supported by the strategic Grant POSDRU/159/1.5/S/133255, Project ID 133255 (2014), co-financed by the European Social Fund within the Sectorial Operational Program Human Resources Development 2007–2013. RUS facilities in Cambridge were established with funding from the Natural Environment Research Council (Grants NE/B505738/1, NE/F017081/1) and from the Engineering and Physical Sciences Research Council (EP/I036079/1).

Appendix

See Table 4.

Table 4 Elastic constants of single-crystal $(Ba_{1-x}Sr_x)_4Na_2Nb_{10}O_{30}$ ($x = 0.3$ and 0.7) solid solutions at RT (from Ref. [59])

Elastic constants, c/N m^{-2}		
c	$Ba_{2.8}Sr_{1.2}Na_2Nb_{10}O_{30}$	$Ba_{1.2}Sr_{2.8}Na_2Nb_{10}O_{30}$
c_{11}	2.268×10^{11}	2.440×10^{11}
c_{22}	2.267×10^{11}	2.440×10^{11}
c_{33}	1.860×10^{11}	1.560×10^{11}
c_{12}	2.120×10^{11}	1.020×10^{11}
c_{13}	1.199×10^{11}	0.740×10^{11}
c_{23}	1.198×10^{11}	0.740×10^{11}
c_{44}	0.607×10^{11}	0.650×10^{11}
c_{55}	0.607×10^{11}	0.650×10^{11}
c_{66}	0.710×10^{11}	0.730×10^{11}

References

1. Eerenstein W, Mathur ND, Scott JF. Multiferroic and magnetoelectric materials. Nature. 2006;442:759–65.
2. Scott JF. Room-temperature multiferroic magnetoelectrics. NPG Asia Mater. 2013;5(11):e72.
3. Salto Y, Takao H, Tani T, Nonoyama T, Takatori T, Homma T, Nagaya T, Nakamura M. Lead-free piezoelectrics. Nature. 2004;432:84–7.
4. Ismailzade IH, Ismailov RM, Alekberov ALI, Salayev FM. Investigation of the magnetoelectric (ME)H effect in solid solutions of the systems $BiFeO_3$-$BaTiO_3$ and $BiFeO_3$-$PbTiO_3$. Phys Status Solidi A. 1981;68:K81–K85.
5. Arnold DC, Morrison FD. B-cation effects in relaxor and ferroelectric tetragonal tungsten bronzes. J Mater Chem. 2009;19:6485–8.
6. Rotaru A, Miller AJ, Arnold DC, Morrison FD. Towards novel multiferroic and magnetoelectric materials: dipole stability in tetragonal tungsten bronzes. Philos Trans R Soc A Math Phys Eng Sci. 2014;372:20120451.
7. Gardner J, Morrison FD. A-site size effect in a family of unfilled ferroelectric tetragonal tungsten bronzes: $Ba_4R_{0.67}Nb_{10}O_{30}$ (R = La, Nd, Sm, Gd, Dy and Y). Dalton Trans. 2014;43:11687–95.
8. Qu W, Tan X, McCallum RW, Cann DP, Ustundag E. Room temperature magnetoelectric multiferroism through cation ordering in complex perovskite solid solutions. J Phys Condens Matter. 2006;18:8935–42.
9. Van Uitert LG, Rubin JJ, Grodkiewicz WH, Bonner WA. Some characteristics of Ba, Sr, Na niobates. Mater Res Bull. 1968;4:63.
10. Van Uitert LG, Levinstein NJ, Rubin JJ, Capio CD, Dearborn EF, Bonner WA. Some characteristics of niobates having 'filled' tetragonal tungsten bronze-like structures. Mater Res Bull. 1968;3:47–57.
11. Wemple SH, DiDomenico M, Camlibel I. Relationship between linear and quadratic electro-optic coefficients in $LiNbO_3$, $LiTaO_3$, and other oxygen-octahedra ferroelectrics based on direct measurement of spontaneous polarisation. Appl Phys Lett. 1968;12:209–11.
12. Jamieson PB, Abrahams SC, Bernstein JL. Ferroelectric tungsten bronze-type crystal structures. I. Barium strontium niobate $Ba_{0.27}Sr_{0.75}Nb_2O_5$. J Chem Phys. 1968;48:5048–57.
13. Jamieson PB, Abrahams SC, Bernstein JL. Ferroelectric tungsten bronze-type crystal structures. II. Barium sodium niobate $Ba(4 + x)Na(2–2x)Nb_{10}O_{30}$. J Chem Phys. 1969;50:4352–63.
14. Cheng TS, Amzallag E, Rokni M. Ferroelectricity measurements on $Sr_xBa_{1-x}Nb_2O_6$. Ferroelectrics. 1972;3:57–8.
15. Zhu XL, Chen XM. Phase transition hysteresis of ferroelectric $Sr_5EuTi_3Nb_7O_{30}$ ceramics with tetragonal tungsten bronze structure. J Appl Phys. 2012;111:044104.
16. Patro PK, Kulkarni AR, Harendranath CS. Microstructure and dielectric properties of strontium barium niobate ceramics synthesized by partial coprecipitation. J Eur Ceram Soc. 2003;23:1329–35.
17. Chandramouli K, Viswarupachary P, Ramam K. Dielectric and pyroelectric properties of monovalent-lithium modified trivalent-samarium doped barium strontium sodium niobate tungsten bronze structured ceramics. J Mater Sci Mater Electron. 2009;20:977–83.
18. Chen XM, Yang JS. Dielectric characteristics of ceramics in BaO–Nd_2O_3–TiO_2–Ta_2O_5 system. J Eur Ceram Soc. 1999;19:139–42.
19. Cao MX, Zhu XL, Liu XQ, Chen XM. Crystal structure and ferroelectric behaviors of $Ba_5SmTi_3Ta_7O_{30}$ and $Ba_4Sm_2Ti_4Ta_6O_{30}$ tungsten bronze ceramics. J Am Ceram Soc. 2010;93:782–6.
20. Miller AJ, Rotaru A, Arnold DC, Morrison FD. Effect of local A-strain on dipole stability in $A_6GaNb_9O_{30}$ (A = Ba, Sr, Ca) tetragonal tungsten bronze relaxor dielectrics. Dalton Trans. 2015;2015(44):10738–45.
21. Ravez J, Simon A. Some solid state chemistry aspects of lead-free relaxor ferroelectrics. J Solid State Chem. 2001;162:260–5.
22. Ravez J, Simon A. Lead-free relaxor ferroelectrics with 'TTB' structure. C R Chimie. 2002;5:143–8.
23. Huang WH, Viehland D, Neurgaonkar RR. Anisotropic glasslike characteristics of strontium barium niobate relaxors. J Appl Phys. 1994;76:490.
24. Liu PP, Zhu XL, Chen XM. Relaxor ferroelectric and magnetic properties of $Ba_6CoNb_9O_{30}$ ceramics with tungsten bronze structure. J Appl Phys. 2009;106:4111.
25. Venet M, M'Peko J-C, Zabotto FL, Guerrero F, Garcia D, Eiras JA. Dynamics of normal to diffuse and relaxor phase transition in lead metaniobate-based ferroelectric ceramics. Appl Phys Lett. 2009;94:172901.
26. Bai Y, Zhu XL, Chen XM, Liu XQ. Dielectric and ferroelectric characteristics of $Ba_5NdFe_{1.5}Nb_{8.5}O_{30}$ tungsten bronze ceramics. J Am Ceram Soc. 2010;93:3573–6.
27. Shvartsman VV, Lupascu DC. Lead-free relaxor ferroelectrics. J Am Ceram Soc. 2012;95:1–26.
28. McCabe EE, West AR. New high permittivity tetragonal tungsten bronze dielectrics $Ba_2LaMNb_4O_{15}$: M = Mn, Fe. J Solid State Chem. 2010;183:624–30.
29. Brandt R, Muller-Buschbaum H. Zur Kristallchemie der tetragonalen Wolframbronze: $Ba_6FeNb_9O_{30}$. Monats Cehm. 1986;117:1239–44.
30. Henshaw GS, Gellman LJ, Williams DE. Selectivity and composition dependence of response of gas-sensitive resistors. Part 1—propane–carbon monoxide selectivity of $Ba_6Fe_xNb_{10}$–xO_{30}($1 \leqslant x \leqslant 2$). J Mater Chem. 1994;4:1427–31.
31. Krainik NN, Isupov VA, Bryzhina MF, Agranovskaya AI. Crystal chemistry of ferroelectrics with structural type of tetragonal oxygen tungsten bronze. Sov Phys Crystallogr. 1964;9:281.
32. Castel E, Josse M, Michau D, Maglione M. Flexible relaxor materials: $Ba_2Pr_xNd_{1-x}FeNb_4O_{15}$ tetragonal tungsten bronze solid solution. J Phys Condens Matter. 2009;21:452201.
33. Josse M, Bidault O, Roulland F, Castel E, Simon A, Michau D, Von der Muhll R, Nguyen O, Maglione M. The $Ba_2LnFeNb_4O_{15}$"tetragonal tungsten bronze": towards RT composite multiferroics. Solid State Sci. 2009;11:1118–23.
34. Castel E, Josse M, Roulland F, Michau D, Raison L, Maglione M. In-situ formation of barium ferrite in iron-doped "tetragonal tungsten bronze": elaboration of room temperature multiferroic composites. J Magn Magn Mater. 2009;321:1773–7.
35. Albino M, Veber P, Pechev S, Labrugere C, Velazquez M, Maglione M, Josse M. Growth and characterization of $Ba_2LnFeNb_4O_{15}$ (Ln = Pr, Nd, Sm, Eu) relaxor single crystals. Cryst Growth Des. 2014;14:500–12.

36. Roulland F, Josse M, Castel E, Maglione M. Influence of ceramic process and Eu content on the composite multiferroic properties of the $Ba_{6-2x}Ln_{2x}Fe_{1+x}Nb_{9-x}O_{30}$ TTB system. Solid State Sci. 2009;11:1709–16.
37. Liu PP, Wu SY, Zhu XL, Chen XM, Liu XQ. Structure, dielectric and magnetic properties of $Ba_6FeNb_9O_{30}$ tungsten bronze ceramics. J Mater Sci Mater Electron. 2011;22:866–71.
38. Damjanovic D. Ferroelectric, dielectric and piezoelectric properties of ferroelectric thin films and ceramics. Rep Prog Phys. 1998;61:1267.
39. Hirota K, Wakimoto S, Cox DE. Neutron and x-ray scattering studies of relaxors. J Phys Soc Jpn. 2006;75:111006.
40. Cross LE. Ferroelectric ceramics: tailoring properties for specific applications. In: Setter N, Colla EL, editors. Ferroelectric ceramics. Basel: Birkhauser; 1993.
41. Rotaru A, Arnold DC, Daoud-Aladine DC, Morrison FD. Origin and stability of the dipolar response in a family of tetragonal tungsten bronze relaxors. Phys Rev B. 2011;83:184302.
42. Rotaru A, Morrison FD. Vogel–Fulcher analysis of relaxor dielectrics with the tetragonal tungsten bronze structure: $Ba_6MNb_9O_{30}$ (M = Ga, Sc, In). J Therm Anal Calorim. 2014;2015(120):1249–59.
43. Carpenter MA. Phase transitions in minerals: strain and elasticity. Eur J Miner. 1998;10:619.
44. Carpenter MA. Static and dynamic strain coupling behaviour of ferroic and multiferroic perovskites from resonant ultrasound spectroscopy. J Phys Condens Matter. 2015;27:263201.
45. McKnight REA. Ph.D. thesis, University of Cambridge, 1999.
46. Nataf GF, Li Q, Liu Y, Withers RL, Driver SL, Carpenter MA. Ferroelastic aspects of relaxor ferroelectric behaviour in $Pb(In_{1/2}Nb_{1/2})O_3$–$Pb(Mg_{1/3}Nb_{2/3})O_3$–$PbTiO_3$ perovskite. J Appl Phys. 2013;113:124102.
47. Maynard J. Resonant ultrasound spectroscopy. Phys Today. 1996;49:26.
48. Migliori A, Maynard J. Implementation of a modern resonant ultrasound spectroscopy system for the measurement of the elastic moduli of small solid specimens. Rev Sci Instrum. 2005;76:121301.
49. Migliori A, Sarrao J. Resonant ultrasound spectroscopy: applications to physics, material measurements and nondestructive evaluation. New York: Wiley; 1997.
50. Farnsworth SM, Kisi EH, Carpenter MA. Elastic softening and polarization memory in PZN-PT relaxor ferroelectrics. Phys Rev B. 2011;84:174124.
51. Carpenter MA, Bryson JFJ, Catalan G, Howard CJ. Elastic and anelastic relaxations in the relaxor ferroelectric $Pb(Mg_{1/3}Nb_{2/3})O_3$: I. Strain analysis and a static order parameter. J Phys Condens Matter. 2012;24:045901.
52. Carpenter MA, Bryson JFJ, Catalan G, Zhang SJ, Donnelly NJ. Elastic and anelastic relaxations in the relaxor ferroelectric $Pb(Mg_{1/3}Nb_{2/3})O_3$: II. Strain–order parameter coupling and dynamic softening mechanisms. J Phys Condens Matter. 2012;24:045902.
53. Carpenter MA, Schiemer JA, Lascu I, Harrison RJ, Kumar A, Katiyar RS, Ortega N, Sanchez DA, Salazar Mejia C, Schnelle W, Echizen M, Shinohara H, Heap AJF, Nagaratnam R, Dutton SE, Scott JF. Elastic and magnetoelastic relaxation behaviour of multiferroic (ferromagnetic + ferroelectric + ferroelastic) $Pb(Fe_{0.5}Nb_{0.5})O_3$ perovskite. J Phys Condens Matter. 2015;27:285901.
54. Pandey CS, Schreuer J, Burianek M, Muhlberg M. Relaxor behavior of $Ca_xBa_{1-x}Nb_2O_6$ ($0.18 \leq x \leq 0.35$) tuned by Ca/Ba ratio and investigated by resonant ultrasound spectroscopy. Phys Rev B. 2013;87:094101.
55. Pandey CS, Schreuer J, Burianek M, Muhlberg M. Anomalous elastic behavior of relaxor ferroelectric $Ca_{0.28}Ba_{0.72}Nb_2O_6$ single crystals. Phys Rev B. 2011;84:174102.
56. Pandey CS, Schreuer J, Burianek M, Muhlberg M. Anomalous elastic behavior of relaxor ferroelectric $Ca_{0.28}Ba_{0.72}Nb_2O_6$ studied by resonant ultrasound spectroscopy. Appl Phys Lett. 2011;99:252901.
57. Pandey CS, Schreuer J, Burianek M, Muhlberg M. Relaxor behavior of ferroelectric $Ca_{0.22}Sr_{0.12}Ba_{0.66}Nb_2O_6$. Appl Phys Lett. 2013;102:022903.
58. Ledbetter HM, Lei M, Hermann A, Sheng Z. Low-temperature elastic constants of $Y_1Ba_2Cu_3O_7$. Phys C. 1994;225:397–403.
59. Jiang W, Cao W, Yi X, Chen H. The elastic and piezoelectric properties of tungsten bronze ferroelectric crystals $(Sr_{0.7}Ba_{0.3})_2NaNb_5O_{15}$ and $(Sr_{0.3}Ba_{0.7})_2NaNb_5O_{15}$. J Appl Phys. 2005;97:094106.
60. McKnight REA, Carpenter MA, Darling TW, Buckley A, Taylor PA. Acoustic dissipation associated with phase transition in lawsonite, $CaAl_2Si_2O_7(OH)_2{\cdot}H_2O$. Am Min. 2007;92:1665–72.
61. McKnight REA, Moxon T, Buckley A, Taylor PA, Darling TW, Carpenter MA. Grain size dependence of elastic anomalies accompanying the α–β phase transition in polycrystalline quartz. J Phys Condens Matter. 2008;20:075229.
62. Migliori A, Darling TW, Baiardo JP, Freibert F. Resonant ultrasound spectroscopy (RUS). In: Levy M, Bass H, Stern R, editors. Handbook of elastic properties of solids, liquids and gases. I. New York: Academic Press; 2001. p. 239–62.
63. Nye JF. Physical properties of crystals. Oxford: Oxford University Press; 1985.
64. Yang B, Li F, Han JP, Yi XJ, Chan HLW, Chen HC, Cao W. Structural, dielectric and optical properties of barium strontium sodium niobate $(Sr_{0.7}Ba_{0.3})_2NaNb_5O_{15}$ single crystals. J Phys D. 2004;37:921.
65. Watt JP. Hashin–Shtrikman bounds on the effective elastic moduli of poly-crystals with orthorhombic symmetry. J Appl Phys. 1979;50:6290–5.
66. Reuss A. Berechnung der Fließgrenze von Mischkristallen auf Grund der Plastizitatsb edingung fur Einkristalle. Z Angew Math Mech. 1929;9:49–58.
67. Voigt W. Lehrbuch der Kristallphysik. Liepzig: Teubner; 1928. p. 962–3.
68. Ledbetter HM. Estimation of Debye temperatures by averaging elastic coefficients. J Appl Phys. 1973;44:1451–4.
69. Hill R. The elastic behaviour of a crystalline aggregate. Proc Phys Soc A. 1952;65:349–54.
70. Ohno I. Free vibration of a rectangular parallelepiped crystal and its application to determination of elastic constants of orthorhombic crystals. J Phys Earth. 1976;24:355–79.
71. Ohno I, Yamamoto S, Anderson OL. Determination of elastic constants of trigonal crystals by the rectangular parallelepiped resonance method. J Phys Chem Solids. 1986;47:1103–8.
72. Demarest HH. Cube-resonance method to determine the elastic constants of solids. J Acoust Soc Am. 1971;49:768–75.
73. Carpenter MA, Salje EKH. Elastic anomalies in minerals due to structural phase transitions. Eur J Min. 1998;10:693–812.
74. Schreuer J, Thybaut T, Prestat M, Stade J, Hausshul E. Towards an understanding of the anomalous electromechanical behavior of langasite and related compounds at high temperatures. In: Proceedings of IEEE ultrasonics symposium 2003. 2003;196–9.
75. Schreuer J, Thybaut T. Anelastic relaxation effects and elastic instabilities in CGG-type compounds. In: Proceedings of IEEE ultrasonics symposium 2005. 2005;695–8.
76. Varshni YP. Temperature dependence of the elastic constants. Phys Rev B. 1970;2:3952.
77. Rotaru A. Ph.D. thesis, University of St Andrews, 2013.
78. Jonscher AK. Dielectric relaxation in solids. London: Chelsea Dielectrics Press; 1983.
79. Donnelly NJ, Bowman RB, Gregg JM. Changes in functional behavior of $93\%Pb(Mg_{1/3}Nb_{2/3})O_3$–$7\%PbTiO_3$ thin films induced by ac electric fields. Phys Rev B. 2006;83:064110.